

SYSTEM MODELING AND IDENTIFICATION OF A PRECISION FAST TOOL SERVO SYSTEM

S. Rakuff¹(student), J. Cuttino¹, D. Schinstock²

¹Mechanical Engr. and Engr. Science, The University of North Carolina at Charlotte, Charlotte, NC 28223

²Dept. of Mechanical Engineering, Tulsa University, Tulsa, OK 74104

Introduction

The Laser industry and the contact lens industry are among many industries to accentuate the need for Fast Tool Servo systems (FTS). FTS's enable diamond turning machines to produce non-axisymmetric components by moving the cutting tool in and out of the workpiece while the spindle rotates. The capability of producing non-axisymmetric parts makes it possible to produce products such as contact lenses for patients with astigmatisms, laser diode corrective lenses, and non-axisymmetric metrology artifacts. Reference [1] for example, utilizes a sinusoidal wave pattern cut along the z-axis of a cylinder to obtain optical instrument transfer functions. With FTS's, the artifact geometry can be expanded to generate periodic, non-axisymmetric waveforms about the rotary axis, thereby enhancing metrology capabilities. The FTS described in this paper is referred to as the *FTSii*. It has an operating frequency of up to 50Hz and a design range of motion of 2mm. The target accuracy is 25nm.

System configuration

The diamond tool is mounted on a monolithic flexure system that is driven by a voice coil actuator. The flexure consists of the tool shuttle, four leaf springs, and two stationary supports. It was machined using a wire EDM to avoid internal stresses. A C-code PID control program runs directly on an Analog Devices Sharc microprocessor mounted on a Precision Micro Dynamics signal processing card. The control loop runs at an interrupt frequency of 40kHz. The voltage signal from the controller is converted into a current by a high bandwidth, high power amplifier. The system is interfaced to the DTM by reading the encoders of the spindle and the x-axis with the DSP-card. An Excel Precision laser interferometer is used to feed back the actual position of the tool shuttle and has 10 nm resolution at a maximum slew rate of 0.7 m/s. Figure 1 illustrates the hardware interaction.

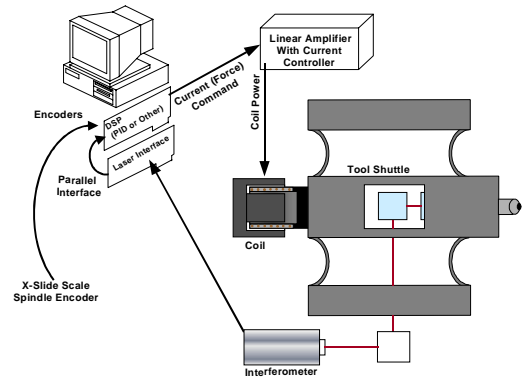


Fig. 1: System configuration

Controller considerations

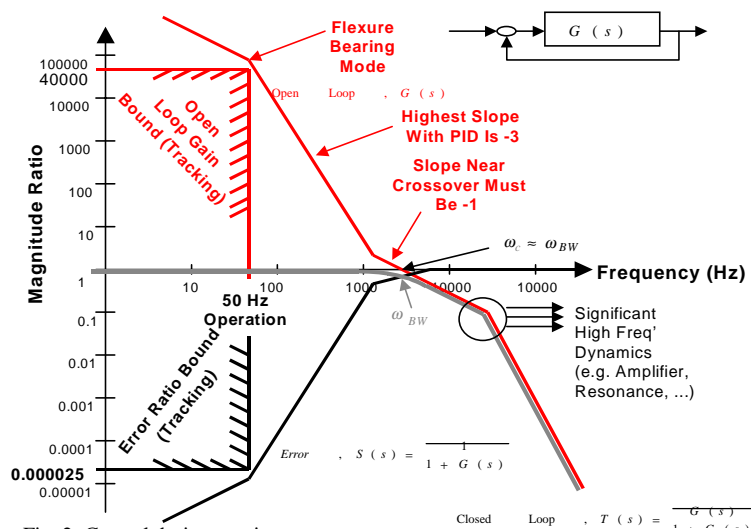


Fig. 2: Control design requirements

Figure 2 shows many of the important aspects of the position control design. Analysis indicates that in order to obtain an error to displacement ratio of 25nm to 1mm at 50 Hz operation of the *FTSii*, a small signal bandwidth of approximately 3 kHz is required for the position control system. This is a design requirement, and has several implications in terms of the mechanical, electrical, and control system designs. The current amplifier/controller for the coil must have a small signal bandwidth of approximately 30 kHz or greater. The mechanical system must not have any resonant modes below 3 kHz other than the main flexure mode that are excited by the actuation force. Finally, the digital position control implementation must have a servo update rate of 30 kHz or greater.

System identification

The system was modeled with the block diagram shown in Figure 3. The model is a time invariant single input single output system. Since the bandwidth of the mechanical system is small compared to the sampling frequency of 40kHz, effects from digital sampling have been assumed to be negligible. The permeability of the coil is assumed to be constant. Under this assumption, the relationship between the current flowing through the coil and the delivered force is linear. The force constant, K_f , is 29.2N/A, and the back-emf constant, K_b , is 21.4Ns/m.

Two possible sources of saturation have significant influence on the performance of the *FTSii*, the DSP card and the amplifier. It is relatively easy to keep the DSP card from saturating by carefully distributing proportional gain among the system components. The amplifier saturates at 8A due to the power supplies and has a maximum slew rate of 8V/ μ s.

The amplifier utilizes a current loop to improve system performance. To decouple the amplifier dynamics and the dynamics of the voice coil from the rest of the system, the bandwidth of the amplifier was designed to be at least one decade higher than the bandwidth of the system. A number of tests were conducted to bring the current loop up to 30kHz, ten times greater than the system's closed loop bandwidth of 3kHz. Therefore, the current loop could be modeled as a constant gain. The quantization effect of the digital laser interferometer and hysteresis of the flexure were also assumed to be negligible. The flexure system was specifically designed to behave as a second order spring mass damper system to optimize the control.

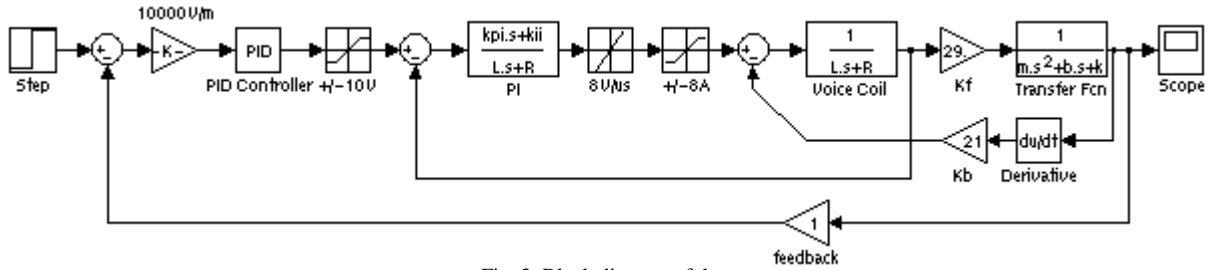


Fig. 3: Block diagram of the system

Determining plant parameters

The moving mass was verified by weighting all moving parts on electronic scales or computed by using dimensional data from the CAD files. In addition, the effective mass was estimated by adding one third of the mass of each leaf spring to the moving mass. The mass was calculated as 1.22 kg (without tool and clamp/bolts). In order to find the damping ratio ζ , the damping b , and the spring constant k , impact testing was performed. Figure 4 shows one set of test data for the first mode. The voice coil was attached to the flexure during testing, since it contributes additional mass and damping caused by Lorenz currents.

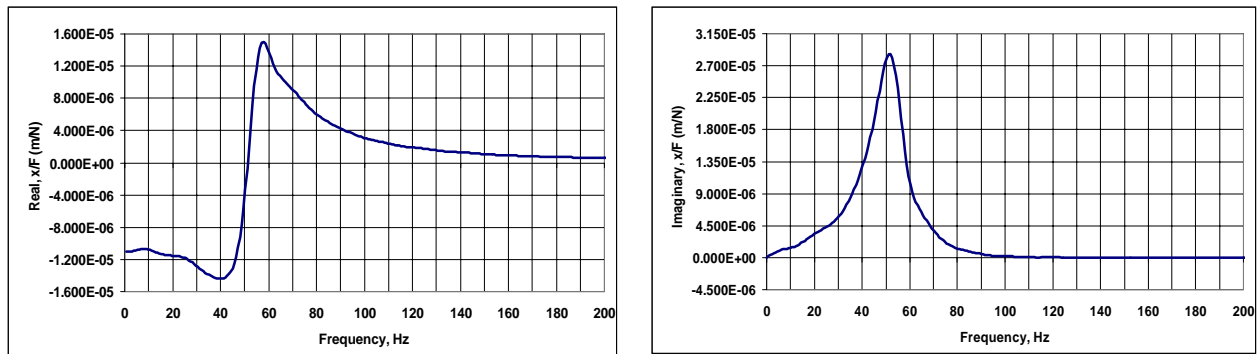


Fig. 4: Fundamental mode frequency response

The two graphs show a damped natural frequency of 53Hz. The damping ratio ζ can be determined by using [3]:

$$\zeta = \frac{\omega_2^2 - \omega_1^2}{4\omega_{dn}^2} \quad (1)$$

The testing for the fundamental mode was repeated several times, resulting in a calculated damping ratio of $\xi = 0.165 \pm 0.002$ (2)

To calculate the undamped natural frequency, the following equations can be used.

$$\omega_n = \frac{\omega_{dn}}{\sqrt{1-\xi}} = \frac{328}{\sqrt{1-0.165}} \text{ rad/s} = 359 \text{ rad/s} \quad (3)$$

The damping, b , of this second order system is equal to

$$b = 2\xi m \omega_n = 144.8 \frac{Ns}{m} \quad (4)$$

For a second order spring mass damper system with no damping, the spring constant k is given as:

$$k = m \omega_n^2 = 1.222 \text{ kg} \cdot (359 \text{ rad/s})^2 = 157492 \frac{N}{m} \quad (5)$$

Tuning the controller

The PID controller for the FTSii was initially designed using the Ziegler-Nichols technique. In this method a unit step is applied to the closed loop system with the controller already installed. Initially, the controller gains, k_p , k_i , and k_d are set to zero. k_p is then increased until the system becomes oscillatory. For the ultimate-cycle method, k_p is then multiplied by 0.6. There are formulas to calculate the other gains with the period of the oscillations [3]. Unfortunately, the limited slew rate of the interferometer (0.7m/s) made it difficult to monitor these oscillations. Since the target applications for the FTSii are sinusoidal, the controller was tuned using a sinusoidal input only. This method is a very general approach and resulted in non-optimal controller gains.

A second approach was applied using Matlab and Simulink simulation packages. The Matlab/Control System toolbox was first used to model the linear system neglecting saturation effects [4]. A PID controller was then designed for this model using the root locus design GUI. The gains were then transferred to an equivalent model created in Simulink and verified. Saturation blocks were then added for DSP card and amplifier.

The transfer function for the PID controller can be written as:

$$TF(s) = k_d s + k_p + \frac{k_i}{s} = \frac{k_d s^2 + k_p s + k_i}{s} = \frac{k_d (s^2 + \frac{k_p}{k_d} s + \frac{k_i}{k_d})}{s} \quad (6)$$

The transfer function introduces two zeroes and one pole at the origin. By selecting a gain and the position of the zeroes, the controller gains were determined. In a first design (Figure 4), the two zeroes and the gain k_d were chosen in such a way that the Bode plot resembled the plot in Figure 2 and Reference [2], with an amplitude ratio of 90dB at 50Hz and crossover at 1500rad/s (2400 Hz). The results are shown in Figure 6.

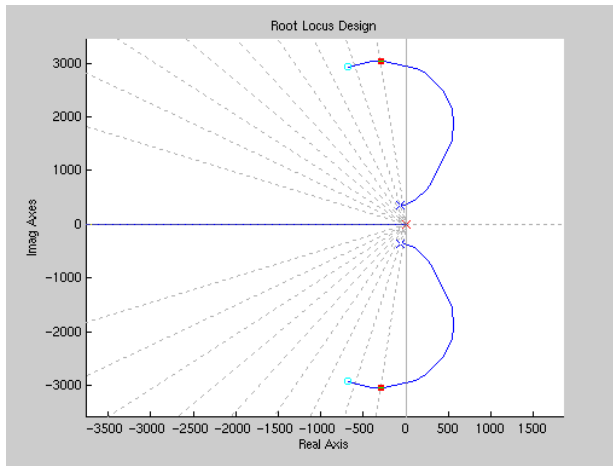


Fig. 5: Root locus of first controller design

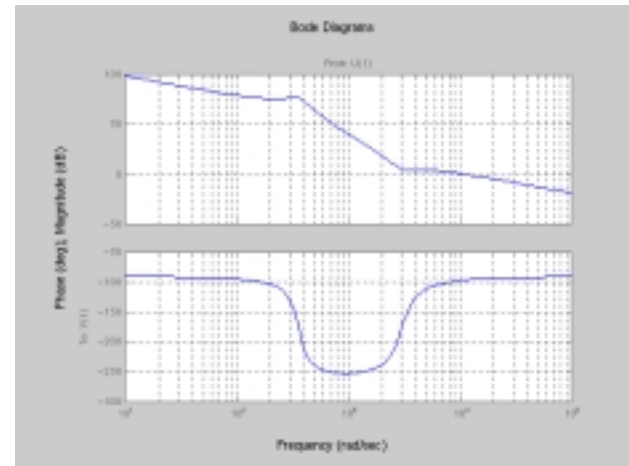


Fig. 6: Bode plot of first controller design

For stability, the phase margin should be greater than 70 degrees. Figure 6 shows that this criterion is met. The transfer function for the controller designed was therefore

$$TF_{PID} = \frac{k_d(s + 669 \pm 2925i)}{s} = \frac{0.05s^2 + 67.51s + 454200}{s}, k_d = 0.05 \text{ sec} \quad (7)$$

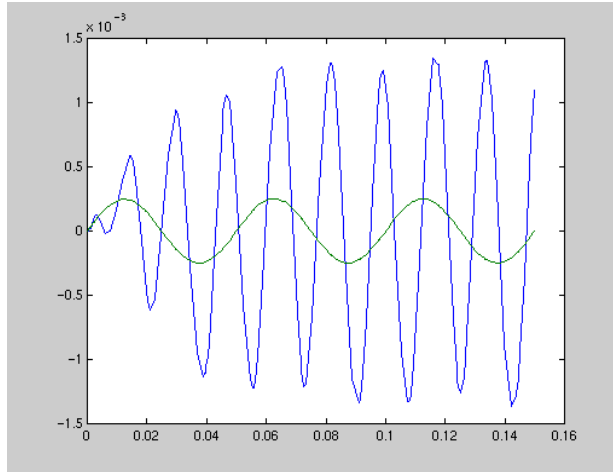


Fig. 7: Unstable system response

The root locus indicates that the derivative gain, k_d , should be greater than 0.02secs or less than $7\mu\text{s}$ for stability. Calculating the controller gains yielded:

$$k_d=0.05\text{sec} \quad k_p = 26513 \quad k_i = 178361240\text{sec}^{-1} \quad (8)$$

The gains were then exported to the Simulink model (Figure 3) to investigate how the non-linearities affected the system. Figure 7 shows the response of the non-linear system to a 20Hz, 250 μm sinusoidal wave. It is obvious that the non-linear system is unstable. The equivalent linear system has minimal error and is stable if the non-linearities are removed.

A possible solution to the problem of saturation is to move the zeros in such a way that the system remains stable even with saturation effects. Figure 8 shows the

zeros in different locations, which led to a new controller design. The Bode plots for this system are shown in Figure 9. The disadvantage of this design is that the crossover frequency is about one order of magnitude higher than in the previous design, thereby requiring a much larger bandwidth of the mechanical system.

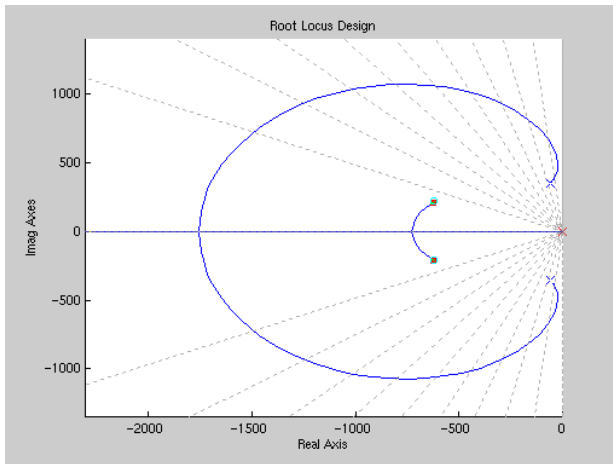


Fig. 8: Loci completely in left hand plane

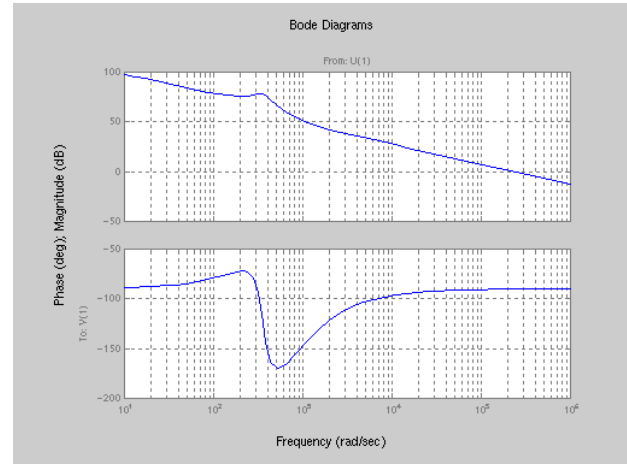


Fig. 9: Bode plot of stable system

The transfer function for this controller was

$$TF_{PID} = \frac{k_d(s + 619 \pm 215i)}{s} = \frac{s^2 + 1238s + 429400}{s} \quad k_d = 1 \quad (9)$$

Calculating the controller gains yielded

$$k_d=1\text{s} \quad k_p=1238 \quad k_i=429400/\text{s} \quad (10)$$

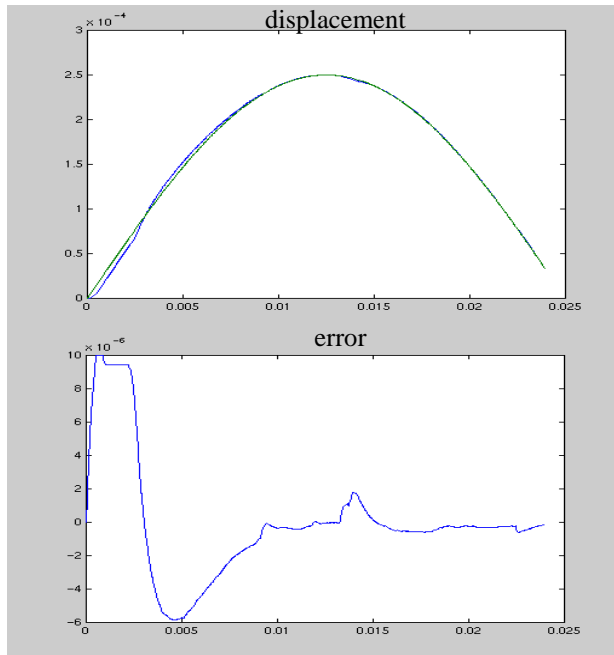


Fig. 10: System response of stable system

These gains were exported into the Simulink model again. From observation it can be seen, that the system has a stable response, even with the presence of saturation (Figure 10). However, the combination of saturation effects and non-optimized gains causes following errors as high as 10 μm . To minimize those errors and to improve the system's performance, the saturation limits need to be raised. At this time, the amplifier is limited to a maximum output of 2A. Once sufficient cooling for the heat sink of the amplifier is achieved, the amplifier should be able to deliver up to 8A.

Conclusion

Once the saturation limits of the amplifier are risen, the following error is expected to drop significantly. Currently, work is being done to interface FTSii with a diamond turning machine. A new housing has been designed that will contain the interferometer, the flexure, and a counterweight to reduce the moment exerted on the slide.

References

1. P. D. Knight, Jr. "Measurement of cylindrical parts by grazing incidence interferometry", Dissertation, University of North Carolina at Charlotte, expected publication September 2000.
2. Guang Lu, "System Identification and Modeling of a Precision Fast Tool Servo", Thesis, University of Alabama, 1999
3. William T. Thomson, Marie Dillon Dahleh, "Theory of Vibration with applications", 5th edition, Prentice Hall, 1998
4. William J. Palm III, "Modeling, Analysis, and Control of Dynamic Systems", 2nd edition, John Wiley and sons, inc.
5. Matlab/Control System Toolbox user's guide, Version 4.2, the Mathworks Inc.

Keywords: Fast Tool Servo, Diamond Turning, PID, Laser Interferometer